Physica Scripta. Vol. T110, 398–402, 2004

Grazing Ion-Surface Collisions

M. S. Gravielle[1]

[1] Instituto de Astronomía y Física del Espacio, CONICET, Casilla de Correo 67, Sucursal 28, 1428, Buenos Aires, Argentina. Also, Dpto. de Física, Universidad Nacional de Buenos Aires.

PACS Ref: 34.50.Dy

Received July 17, 2003; accepted November 4, 2003

Abstract

Electron emission after grazing ion-surface collisions is studied for high impact velocities. We have focused on glancing angles of electron emission where the dominant mechanism is the ionization from atomic bound states. To describe this process, we introduce a quantum model called field distorted-wave (FDW) approximation, which takes into account the effect of the surface interaction on the electronic transition.

The FDW model is applied to analyze electron distributions produced by impact of protons on Al and LiF surfaces, which are metal and insulator materials respectively. In the case of metals, we also evaluate the contibution coming from the valence band by employing the binary collisional formalism. Calculated electron emission yields are in reasonable agreement with the available experimental data. We find that the maximum of the convoy electron distribution is *accelerated* for Al and *decelerated* for LiF, with respect to its position in ion-atom collisions, in quantitative accordance with experiments.

1. Introduction

Electron emission produced during the grazing scattering of ions from solid surfaces has been the subject of intense experimental and theoretical research in the last ten years [1–11]. The interest in such an inelastic process has been motivated by the particular features of the collisional system, which allows us to extract specific information about the chemical and topographic composition of the surface from the electron distributions. Depending on the charge state and the velocity of the incident ion, different phenomena are involved in the ejection of electrons from surfaces. A complete review of these processes can be found in Ref. [12] and references inside.

At high impact velocities, the charge state of the ion can be considered as fixed [13,14], and one of the most interesting regions of electron observation angles is around the direction of specular reflection of the projectile. In this angular region, the energy distribution of the emitted electrons displays a prominent structure, usually named convoy electron peak (CEP), whose shape and position differ markedly from that observed in ion-atom collisions. While for gaseous targets the CEP looks like a cusp-shaped peak at electron velocities that match the projectile velocity, for collisions involving solid surfaces the peak appears appreciably shifted and broadened. And both features are a direct consequence of the presence of an effective surface interaction, as earlier proposed by Burgdörfer [3]. In the theoretical field, Burgdörfer and Reinhold [4,5] were the first ones to tackle the problem within the framework of the classical trajectory Monte Carlo approach.

In the present work, we study the energy distribution of electrons originated by grazing impact of fast protons on surfaces, considering two different materials: metals and insulators. The focus of interest is the forward direction, where the electron emission is primarily due to direct ionization of surface atoms. Our intention is to investigate the performance of a recently proposed method, called *field distorted-wave* (FDW) approximation [15]. It is an extension of the continuum-distorted-wave-eikonal-initial-state (CDW-EIS) approximation, which allows us to describe the ionization from atomic bound states taking into account the influence of the surface electric field. The final goal is to get information about the surface potentials from electron spectra. Throughout this article, atomic units are used unless otherwise stated.

2. Electron emission from atomic bound states

In collisions involving surfaces, the ionization of the surface atoms develops in the presence of the potential V_0 originated by the solid medium. In the case of metals, V_0 represents the surface induced potential, while for insulators it also includes the track potential produced by the target ionization along the ion path. We employ the *field-distorted-wave* (FDW) approximation to evaluate the electron emission from atoms situated at the topmost atomic layer. The physics underlying the FDW model can be outlined as follows: Due to the nearness of the solid, the active electron feels the action of the surface field, $\boldsymbol{E}_0(\boldsymbol{r}, t) = -\nabla_{\boldsymbol{r}} V_0(\boldsymbol{r}, t)$. Within the FDW approximation, the effect of the field $\boldsymbol{E}_0$ on the evolution of the electronic state, before and after the collision, is described with the Volkov anzats [16], while the electronic transition, produced during the close interaction with the projectile, is represented with a CDW-EIS-type theory [17].

In the FDW model, the T-matrix element, $\mathcal{T}_{if}^{\mathrm{FDW}}$, corresponding to the transition from the initial atomic state i to the final state f, with momentum $\boldsymbol{k}_f$, is expressed in terms of analytical Nordsieck integrals (see Ref. [15] for details). An approximated expression of $\mathcal{T}_{if}^{\mathrm{FDW}}$ is given by

$$\mathcal{T}_{if}^{\mathrm{FDW}} \simeq \frac{F_P^{(s)-*}(k_P)}{F_P^{-*}(|\boldsymbol{k}_f - \boldsymbol{v}|)} \frac{F_T^{-*}(k_T)}{F_T^{-*}(k_f)} \mathcal{T}_{if}^{\mathrm{CDW-EIS}}, \tag{1}$$

where $\mathcal{T}_{if}^{\mathrm{CDW-EIS}}$ denotes the transition matrix calculated with the usual CDW-EIS approximation [17], and F_c^- is the well-known Coulomb Jost function,

$$F_c^-(k) = \exp\left(\frac{\pi Z_c}{2k}\right)\Gamma(1 + \mathrm{i}Z_c/k), \qquad c = P, T, \tag{2}$$

with $Z_P(Z_T)$ the charge of the projectile (target nucleus) and $\boldsymbol{v}$ the projectile velocity. The function $F_P^{(s)-}(k)$ is

determined by the effective projectile potential and depends on the electronic structure of the surface. In insulator surfaces, as the mobility of valence electrons is weak, the projectile interaction can be represented by a *pure* Coulomb potential, the function $F_P^{(s)-}$ being defined as $F_P^{(s)-}(k) = F_P^-(k)$. For metals, instead, the projectile is shielded by valence electrons, and $F_P^{(s)-}(k)$ represents the Jost function corresponding to the potential $V_P^{(s)} = -Z_P \exp(-\lambda r)/r$, which is used to describe the dynamic screening of the incident ion. The parameter λ is fixed as $\lambda = w_s\,(v^2 + v_F^2/3)^{-1/2}$, with w_s the surface plasmon frequency and v_F the Fermi velocity.

The vectors $\boldsymbol{k}_P$ and $\boldsymbol{k}_T$, involved in Eq. (1), are the electron momenta with respect to the projectile and to the target nucleus respectively, just after the atomic collision. They are related to the final electron momentum measured by the detector, $\boldsymbol{k}_f$, by:

$$\boldsymbol{k}_T = \boldsymbol{k}_f + \boldsymbol{A}_f(x), \qquad \boldsymbol{k}_P = \boldsymbol{k}_f - \boldsymbol{v} + \boldsymbol{A}_f(x), \tag{3}$$

where $\boldsymbol{A}_f$ is a supplementary transferred momentum introduced by the field $\boldsymbol{E}_0$. From the electromagnetic point of view, the vector

$$\boldsymbol{A}_f(x) = -\left(\frac{d_s}{2}\right)\frac{\boldsymbol{E}_0(\boldsymbol{R}(x), x/v)}{v} \tag{4}$$

represents the vector potential of the surface field acting on the emitted electron. It depends on the projectile position $\boldsymbol{R}(x) \equiv (x, Z(x))$, where x and $Z(x)$ are the components of $\boldsymbol{R}$ parallel and perpendicular to the surface respectively, with $Z(x)$ the classical projectile trajectory. In Eq. (4), $\boldsymbol{E}_0$ is evaluated at the time $t = x/v$ when the atomic collision takes place and d_s denotes an effective collisional distance.

By employing a frame of reference fixed to the atomic surface, with the projectile trajectory contained in the plane $\hat{x} - \hat{z}$ and the surface in the plane $\hat{x} - \hat{y}$, the final electron momentum reads $\boldsymbol{k}_f = k_f(\cos\theta_e \cos\phi_e, \cos\theta_e \sin\phi_e, \sin\theta_e)$. The angle θ_e represents the elevation angle with respect to the surface and ϕ_e is the angle between the direction of emission and the scattering plane, measured on the surface plane.

3. Results for metal surfaces

The study on metal surfaces is confined here to 100 keV-protons impinging on an Al(111) surface with a glancing incidence angle ($\theta_i = 1^\circ$). For this collisional system, recent experimental spectra have been published [18]. In metals, the surface field is originated by the *induced potential* associated with the dielectric response of the material. We employ the specular-reflection (SR) model [19] to describe the electric field $\boldsymbol{E}_0$ induced by the projectile. Although the surface field should also include the self-image field induced by the ionized electron, its contribution can be neglected, as explained in Ref. [18].

We start the analysis investigating the main features of the convoy electron emission. At the ejection angle ($\theta_e = 1^\circ, \phi_e = 0^\circ$)—which coincides with the direction of the outgoing projectile—the CEP is the most striking structure in the electron spectrum. Within the FDW model, the behavior of the atomic ionization probability around

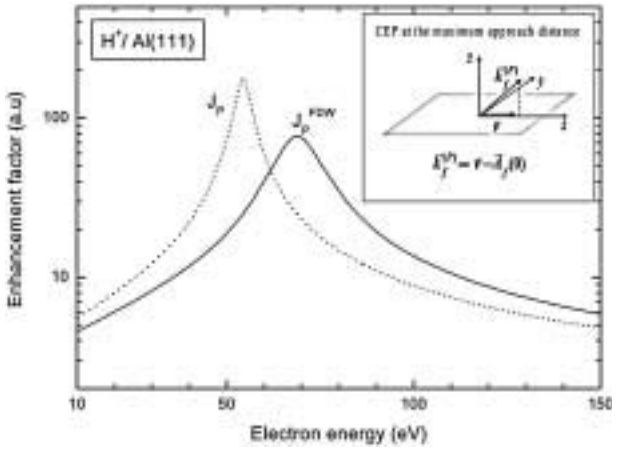

Fig. 1. Enhancement factor involved in the calculation of the atomic ionization probability, as a function of the final electron energy, for 100 keV-protons colliding with an Al(111) surface with the incidence angle $\theta_i = 1^\circ$. The projectile is considered at the closest distance to the surface and the electron emission angle is ($\theta_e = 1^\circ, \phi_e = 0^\circ$). Solid line, function $J_P^{\mathrm{FDW}}(\boldsymbol{k}_f)$, as defined by Eq. (5); dotted line, enhancement factor in absence of the surface interaction, $J_P(\boldsymbol{k}_f) = |F_P^-(|\boldsymbol{k}_f - \boldsymbol{v}|)|^2$. A schematic drawing of the position of the CEP in the final momentum space is shown in the inset.

the CEP is determined by the Jost function $F_P^{(s)-}(k_P)$, which presents a maximum for $k_P \to 0$. In Fig. 1, we show the absolute value of $F_P^{(s)-}(k_P)$,

$$J_P^{\mathrm{FDW}}(\boldsymbol{k}_f) = \left|F_P^{(s)-}(k_P)\right|^2, \tag{5}$$

with $\boldsymbol{k}_P = \boldsymbol{k}_f - \boldsymbol{v} + \boldsymbol{A}_f(x)$, considering the projectile at the closest distance to the surface, which is reached as $x = 0$. The Jost function in absence of the surface interaction, $J_P(\boldsymbol{k}_f) = |F_P^-(|\boldsymbol{k}_f - \boldsymbol{v}|)|^2$, is also plotted in the figure for comparison. The enhancement factor J_P^{FDW}, defined by Eq. (5), dominates the energy spectrum obtained with the FDW approximation in the region of the convoy electron emission. It displays a peak for values of the final electron momentum $\boldsymbol{k}_f$ close to $\boldsymbol{k}_f^{(P)} = \boldsymbol{v} - \boldsymbol{A}_f(x)$, with $k_{fz}^{(P)} = -A_{fz}(x) > 0$, which corresponds to electrons ejected almost parallel to the surface. And this peak does not present the cusp shape characteristic of Coulomb interactions, observed in J_P. In metals, the induced field $\boldsymbol{E}_0$ is essentially responsible for the displacement of the maximum of J_P^{FDW} towards higher energies, while the widening of the peak is mainly due to the shielding of the projectile, included in the potential $V_P^{(s)}$ [15]. Note that the function J_P^{FDW} displayed in Fig. 1 must be then integrated along the projectile trajectory, giving rise to a small additional broadening of the convoy structure.

In order to compare with experimental electron distributions, we also evaluate the contribution coming from the valence band of the metal. The ionization of valence electrons, which form the surface free-electron gas, is calculated within the binary collisional formalism, using the *modified specular reflection* (MSR) model to represent the surface wake potential [20]. The plasmon decay mechanism is not included in the calculations because it only contributes for low electron energies [21], not considered here. Differential probabilities of electron emission are shown in Fig. 2, for two electron observation

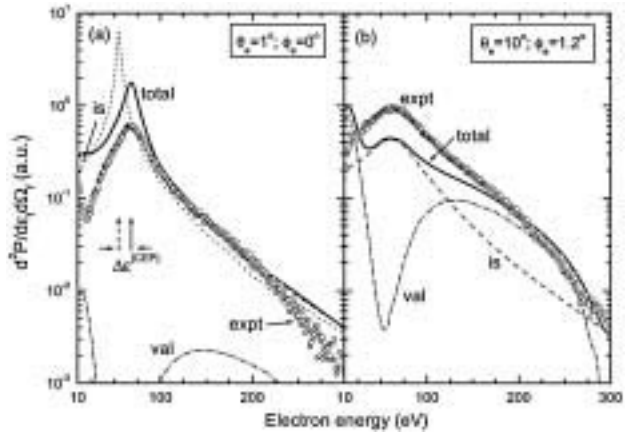

Fig. 2. Differential probability of electron emission, $d^2P/d\varepsilon_f d\Omega_f$, for 100 keV-protons impinging on an Al(111) surface with the incidence angle $\theta_i = 1^\circ$. The electron emission angles are: (a) $(\theta_e = 1^\circ, \phi_e = 0^\circ)$, and (b) $(\theta_e = 10^\circ, \phi_e = 1.2^\circ)$. Empty circles, normalized experimental data of Ref. [18]. Theoretical predictions: solid line, total probability of electron emission calculated by adding inner-shell (FDW model) and binary valence contributions; dashed (dotted) line, inner-shell emission probability calculated with (without) including the surface interaction; dashed-dotted line, valence emission probability. The symbol $\Delta\varepsilon^{(CEP)}$ denotes the energy shift of the CEP, with respect to its position for $\boldsymbol{E}_0 = \boldsymbol{0}$.

angles: $(\theta_e = 1^\circ, \phi_e = 0^\circ)$ and $(\theta_e = 10^\circ, \phi_e = 1.2^\circ)$. Our total predictions were obtained by adding core and valence contributions, which are also plotted in the figure to display the electron energy range where each process is relevant. Experiments extracted from Ref. [18] are normalized with the theory.

As mentioned above, for the angle $\theta_e = 1^\circ$, the presence of the convoy structure dominates the shape of the experimental and theoretical spectra. At this electron emission angle, the inner-shell ionization is more than one order of magnitude higher than the valence contribution in the whole electron energy range. And in particular, for electron energies around the CEP, the emission of valence electrons is *not* possible by binary collisions. It is due to the fact that the values of $\boldsymbol{k}_f$ reached by the mechanism of binary ionization from the valence band are confined in the region $K_{\min} \leq |\boldsymbol{k}_f - \boldsymbol{v}| \leq K_{\max}$, as a consequence of the energy conservation [22]. The limits of this area in the momentum space are $K_{\min} = [(v - v_F)^2 - k_c^2]^{1/2}\ \Theta[v - (k_c + v_F)]$ and $K_{\max} = [(v + v_F)^2 - k_c^2]^{1/2}$, with $k_c = (2E_W + v_F^2)^{1/2}$, E_W the work function, and Θ the unitary Heaviside function.

The general characteristics of the experimental spectrum displayed in Fig. 2(a) are well described by the FDW approximation. The model predicts an energy shift of the CEP (defined as the difference between the positions of the maximum of the energy distribution with and without including $\boldsymbol{E}_0$) $\Delta\varepsilon^{(CEP)} \simeq 13.5$ eV, which is quite similar to the experimental value $\Delta\varepsilon^{(CEP)}_{\text{exptt}} \simeq 14.5$ eV [18].

When the electron path departs from the forward direction, the valence emission increases and the ionization from atomic bound states diminishes. For the angle $\theta_e = 10^\circ$, shown in Fig. 2(b), the theoretical spectrum shows the footprints of both, the CEP and the *binary ridge*, coming from the inner-shell and valence contributions respectively. At this emission angle, theoretical results coincide with the experimental data for high electron energies, but around the projection of the CEP, the theory underestimates the experiment. Such a discrepancy could be a consequence of the presence of other mechanisms not included in the model.

Finally, in spite of the reasonable agreement found with experiments, we should add that for metals, the electrons ionized with $\theta_e = 1^\circ$ travel a long distance through the jellium before being emitted to the vacuum region, suffering multiple collisions in the outgoing path. This effect (transport) has not been included in the theoretical model. Then, the theoretical probabilities shown in Fig. 2(a) correspond to the *primary* electron distribution that is obtained by considering that ionized electrons are directly ejected to the vacuum. For larger θ_e, instead, the path of emitted electrons inside the jellium decreases rapidly, and the primary distribution displayed in Fig. 2(b) can be directly compared with the observable spectrum.

4. Results for insulator surfaces

As an example of collision with insulator materials, we consider the system composed by 100 keV-protons impinging on an LiF(100) surface with the incidence angle $\theta_i = 0.7^\circ$. At this impact energy, emitted electrons come mainly from bound states to F^- target ions.

In insulator surfaces, due to the low conductivity of the medium, the ionization of the target along the projectile path originates a surface charge density which is responsible for the track potential. We consider, as a first estimate, that the *track potential* represents the dominant surface interaction that affects the movement of emitted electrons [8,11], and the dielectric response of the medium is weak in comparison with it [23]. In this work, the track field has been derived from the CDW-EIS approximation, without including the shielding originated by slow ionized electrons [24].

We consider a small emission angle, $\theta_e = 0.7^\circ$, for which the CEP is the most noticeable structure of the electron distribution. As in the previous Section, to analyze the effect of the surface field on convoy electrons, in Fig. 3 we plot the enhancement factor J_P^{FDW}, given by Eq. (5), when the projectile is at the distance of maximum approach to

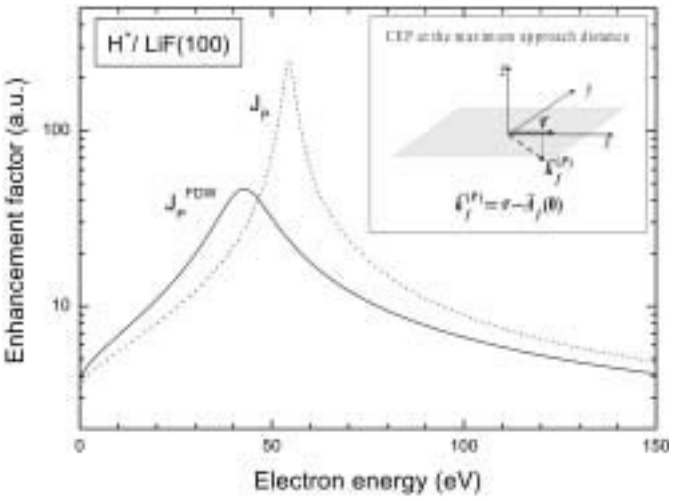

Fig. 3. Similar to Fig. 1 for 100 keV-protons colliding with a LiF(100) surface with the incidence angle $\theta_i = 0.7^\circ$. The electron observation angle is $(\theta_e = 0.7^\circ, \phi_e = 0^\circ)$.

the surface. The function $J_P = |F_P^-(|\boldsymbol{k}_f - \boldsymbol{v}|)|^2$, corresponding to $\boldsymbol{E}_0 = \boldsymbol{0}$, is again shown as a reference. Although for insulators the projectile interaction is represented by a Coulomb potential, the function J_P^{FDW} does not display the typical Coulomb divergent shape around the maximum. We observe that, as a result of the additional momentum transfer $\boldsymbol{A}_f$, the maximum of J_P^{FDW} is energy displaced and lowered. This last effect is because the Coulomb peak of J_P^{FDW} as $k_P \to 0$ is now centered on the position $\boldsymbol{k}_f^{(P)} = \boldsymbol{v} - \boldsymbol{A}_f(x)$, with $k_{fz}^{(P)} = -A_{fz}(x) < 0$, in the final momentum space, which corresponds to electrons emitted inside the solid, not detected in experiments. Therefore, the action of track field on ionized electrons produces not only the energy shift but also the broadening of the convoy structure. Besides, the form of the total spectrum is obtained by integrating the ionization probability on the projectile path, which widens the peak even more.

In Fig. 4 we plot the differential probability of electron emission along the direction of specular-reflection of the projectile, i.e. $(\theta_e = 0.7^\circ, \phi_e = 0^\circ)$. Results of the FDW model are compared with the ones obtained by considering the track potential equal to zero. The FDW energy distribution shows a convoy structure that is remarkably broadened and shifted towards a lower energy. The theory provides an energy shift of the convoy peak $\Delta\varepsilon^{(CEP)} \simeq -4\,\mathrm{eV}$, which is close to the experimental value $\Delta\varepsilon_{\mathrm{exp\,t}}^{(CEP)} \simeq -5\,\mathrm{eV}$ [8]. Even though experiments for these high impact velocities are not available, the shape of the electron distribution qualitatively agrees with experimental spectra obtained for lower projectile energies [8].

Note that, unlike what happens with metals, in insulator surfaces the electrons emitted in all the directions can be supposed as being directly ejected to the vacuum semi-space. The FDW model seems to give an appropriate description of the broadening and the energy shift of the CEP, which are the signs of the presence of the track potential. However, there are other effects not included in our calculations, like screening by low energy electrons or polarization of the surrounding anions, that might strongly reduce the strength of the track potential, attenuating the influence of this potential on electron emission spectra. Calculations to take into account these processes are being carried out.

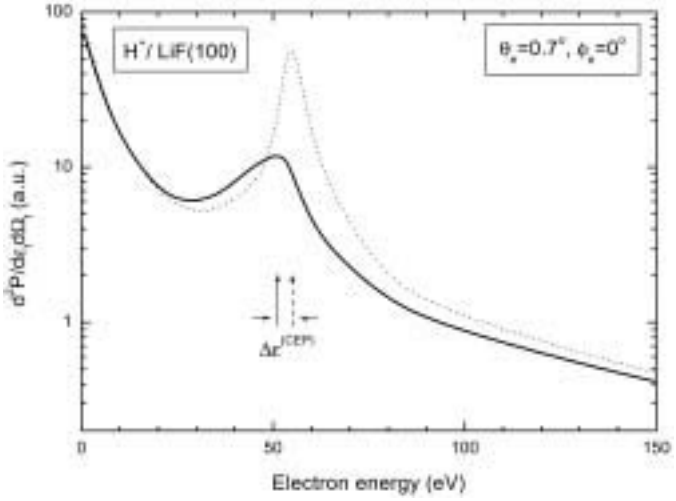

Fig. 4. Differential probability of electron emission from bound states to target ions, $\mathrm{d}^2P/\mathrm{d}\varepsilon_f\,\mathrm{d}\Omega_f$, for 100 keV-protons impinging on a LiF(100) surface with the incidence angle $\theta_i = 0.7^\circ$. The electron ejection angle is $(\theta_e = 0.7^\circ, \phi_e = 0^\circ)$. Solid line, results obtained with the FDW approximation; dotted line, values from the CDW-EIS approximation, without including the surface interaction.

5. Conclusions

We have presented a theoretical model to describe the angle and energy distributions of electrons emitted during the grazing impact of fast protons on solid surfaces. We have concentrated on the description of the ionization process from atomic bound states, for which a quantum model named FDW approximation has been proposed. Within the FDW approach, the presence of the solid medium introduces an additional transferred momentum $\boldsymbol{A}_f$, which depends on the surface field at the different positions of the projectile.

In order to investigate the role played by electronic characteristics of the surface, we have applied the model to collisions with Al and LiF, which are metal and insulator respectively. For aluminum surfaces, we have also calculated the electron emission from the valence band (free-electron gas) by using the binary collisional formalism, with the surface induced potential given by the MSR model. Energy distributions for different angles of electron emission were found in reasonable agreement with the available experimental spectra. In the forward direction, the FDW model predicts an energy shift and broadening of the CEP, that are confirmed by experiments for both, Al and LiF surfaces. However, in the case of insulators an exhaustive experimental study should be useful to analyze the relative importance of the different surface interactions. It would allow us to verify the validity of the proposed model for a wider range of electron observation angles.

Acknowledgments

The author gratefully acknowledges J. E. Miraglia for helpful and stimulating discussions and collaboration. The author also would like to thank G. G. Otero, E. A. Sánchez, O. Grizzi, A. Arnau and V. H. Ponce for fruitful collaborations. This work was supported in part by the ANPCyT (projects No. PICT 03-03579 and No. PICT03-06249) and UBACyT (project No. X044).

References

1. Kimura, K., Tsuji, M. and Mannami, M., Phys. Rev. A **46**, 2618 (1992).
2. Thumm, U., J. Phys. B **25**, 421 (1992).
3. Burgdörfer, J., "Progress in Atomic and Molecular Physics," (Edited by C. D. Lin) (World Scientific Publ., 1993).
4. Reinhold, C. O., Burgdörfer, J., Kimura, K. and Mannami, M., Phys. Rev. Lett. **73**, 2508 (1994).
5. Reinhold, C. O. and Burgdörfer, J., Phys. Rev. A **55**, 450 (1997).
6. Gómez, G. R., Sánchez, E. A., Grizzi, O., Martiarena, M. L. and Ponce, V. H., Nucl. Instr. Meth. B **122**, 171 (1997).
7. Minniti, R., Elston, S. B., Reinhold, C. O., Lim, J. Y. and Burgdörfer, J., Phys. Rev. A **57**, 2731 (1998).
8. Gómez, G. R., Grizzi, O., Sánchez, E. A. and Ponce, V. H., Phys. Rev. B **58**, 7403 (1998).
9. Kimura, K., Andou, G. and Nakajima, K., Nucl. Instr. Meth. B **164–165**, 933 (2000).
10. Gravielle, M. S., Phys. Rev. A **62**, 062903 (2000).
11. Kimura, K., Usui, S., Maeda, K. and Nakajima, K., Nucl. Instr. Meth. B **193**, 661 (2002).
12. Winter, H., Phys. Reports **367**, 387 (2002).
13. Miraglia, J. E., Phys. Rev. A **50**, 2410 (1994).

14. Gravielle, M. S. and Miraglia, J. E., Phys. Rev. A **50**, 2425 (1994).
15. Gravielle, M. S. and Miraglia, J. E., Phys. Rev. A **67**, 042901 (2003).
16. Volkov, D. M., Z. Phys. **94**, 250 (1935).
17. Fainstein, P. D., Ponce, V. H. and Rivarola, R. D., J. Phys. B **21**, 287 (1988).
18. Gravielle, M. S., Miraglia, J. E., Otero, G. G., Sánchez, E. A. and Grizzi, O., to be published, Phys. Rev. A (2004).
19. García de Abajo, F. J. and Echenique, P. M., Phys. Rev. B **46**, 2663 (1992).
20. Gravielle, M. S. and Miraglia, J. E., Phys. Rev. A **65**, 022901 (2002).
21. Sánchez, E. A., Gayone, J. E., Martiarena, M. L., Grizzi, O. and Baragiola, R. A., Phys. Rev. B **61**, 14 209 (2000).
22. Gravielle, M. S., Phys. Rev. A **58**, 4622 (1998).
23. Miraglia, J. E. and Gravielle, M. S., Phys. Rev. A **67**, 062901 (2003).
24. Arnau, A., Gravielle, M. S., Miraglia, J. E. and Ponce, V. H., Phys. Rev. A **67**, 062902(2003).